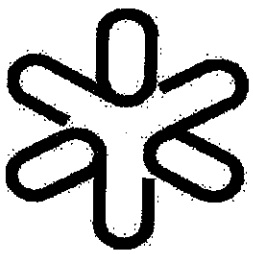

Instituto de Física
Universidade de São Paulo

RADIATION REACTION EFFECTS IN THE STERN-GERLACH DEVICES

Blanco, R.
Universidade de Cantabria, Santander, Spain
Dechoum, K; França, H. M.; Sponchiado, R. C.
Instituto de Física, Universidade de São Paulo, SP, Brasil

Publicação IF - 1393/99

RADIATION REACTION EFFECTS IN THE STERN-GERLACH DEVICES

R. Blanco[1], K. Dechoum[2], H.M. França*[2] and R.C. Sponchiado[2]

1. Universidad de Cantabria, 39005 Santander, Spain
2. Instituto de Física, Universidade de São Paulo, C.P. 66318, 05315-970 São Paulo, SP, Brazil

ABSTRACT

We give a detailed analysis of the dynamical effects of the radiation reaction forces, acting in the magnetic deflection of an atomic beam characteristic of the Stern-Gerlach type experiments. We show that the incident atomic beam is splitted in two beams by the action of the radiation reaction torque. This phenomenon is, however, dynamically different from the standard Stern-Gerlach effect because the space variation, and the total magnitude of the magnetic field, are equally important. The strong dependence of the beam splitting on the total magnitude of the field, is characteristic of the processes of emission of radiation because the Larmor formula is proportional to the fourth power of the Larmor frequency. We suggest experiments to test our theoretical predictions.

*Corresponding author, e-mail: hfranca@if.usp.br

1. INTRODUCTION

In a recent publication a successful classical analysis of the Stern-Gerlach phenomenon was discussed in detail [1]. According to Dechoum, França and Malta, the Pauli-Schrödinger equation is closely related to the Liouville equation, and this fact allowed then to give an adequate classical description of the Stern-Gerlach type experiments, by treating satisfactorily the non-linear magnetic forces acting on the atoms, and considering continuous orientation angles of the magnetic dipole.

In this paper we shall give further attention to the classical aspects of the Stern-Gerlach phenomenon, by studying the dynamical role of the radiation reaction forces acting on the magnetic particles of the beam. Our starting point is similar to that discussed by A.F. Rañada and M.F. Rañada [2], in the interesting paper entitled "The Stern-Gerlach quantum-like behaviour of a classical charged particle". There are, however, some important differences which are clarified in our Section 2.

In order to identify clearly the role of the radiation reaction forces, the conventional Stern-Gerlach effect (quantum or classical) is neglected in our theoretical calculations. This will be very useful because we shall see that the effects of the radiation reaction torque are very similar to the conventional Stern-Gerlach phenomenon. We will show that this procedure enable us to identify the signature of the radiation reaction forces acting on the magnetic particles.

Our paper is organized as follows. We first give a summary of the derivation of the radiation reaction torque acting on the electron, emphasizing the application to the magnetic deflection of neutral atoms in the Stern-Gerlach type devices. The splitting of the Maxwell-Boltzmann velocity distribution is discussed in the Section 3. Within Section 4 we calculate the distribution of particles on a distant screen. We show that the incident beam is splitted in two beams whose separation presents a

characteristic dependence on the total magnitude of the applied magnetic field. Finally, our conclusions are summarized in Section 5.

2. RADIATIVE CORRECTIONS TO THE LARMOR PRECESSION

The large magnetic moment of a neutral atom is generated by the electron and it is given by

$$\boldsymbol{\mu} = \frac{-e\,g\,\boldsymbol{S}}{2mc} \ , \tag{1}$$

where $-e$ is the electron charge, m is the electron mass, c is the velocity of light, $\boldsymbol{S}$ is the electron spin vector and g is the intrinsic gyromagnetic factor ($g \simeq 2$ for electrons [3]). Let us first consider the case of a single (isolated) electron.

Under the action of a constant magnetic field $\boldsymbol{B}$, the magnetic electron precesses with the Larmor frequency $\omega = e|\boldsymbol{B}|/mc$ as indicated in the Fig. 1. The electric and magnetic fields generated by the precessing electron, located at the origin of the coordinate system, are such that [4]

$$\boldsymbol{E}_e \ \simeq \ \frac{-e\widehat{\boldsymbol{n}}}{r^2} + \frac{\widehat{\boldsymbol{n}} \times \dot{\boldsymbol{\mu}}}{c\,r^2} + \frac{\widehat{\boldsymbol{n}} \times \ddot{\boldsymbol{\mu}}}{c^2\,r} \ , \tag{2}$$

$$\boldsymbol{B}_e \ \simeq \ \frac{3\,\widehat{\boldsymbol{n}}\,(\widehat{\boldsymbol{n}} \cdot \boldsymbol{\mu}) - \boldsymbol{\mu}}{r^3} + \frac{3\,\widehat{\boldsymbol{n}}\,(\widehat{\boldsymbol{n}} \cdot \dot{\boldsymbol{\mu}}) - \dot{\boldsymbol{\mu}}}{c\,r^2} + \frac{\widehat{\boldsymbol{n}} \times (\widehat{\boldsymbol{n}} \times \ddot{\boldsymbol{\mu}})}{c^2\,r} \ , \tag{3}$$

where $\widehat{\boldsymbol{n}} = \boldsymbol{r}/r$ and the vector $\boldsymbol{\mu}$ is a function of the retarded time $t - r/c$.

These fields generates in space surrounding the electron, an electromagnetic angular momentum (or spin) which is given by [4]

$$\boldsymbol{S}_e = \int d^3r\, \frac{\boldsymbol{r}}{4\pi c} \times (\boldsymbol{E}_e \times \boldsymbol{B}_e) \ . \tag{4}$$

This quantity is divergent for a point-like electron. However, from the old classical electron model of Abraham and Lorentz [5,6], and also from the modern QED picture [7], it

has been proposed that the electron is an extended charge, with a radius R estimated to vary from e^2/mc^2 (classical electron radius) to $\hbar/mc$ (Compton radius) approximately. In this regard, it is interesting to calculate $\boldsymbol{S}_e$ using the first terms in (2) and (3), assuming $R = e^2/mc^2$ and by considering the experimental value $|\boldsymbol{\mu}| = e\hbar/2mc$. The calculation is straightforward and leads to $|\boldsymbol{S}_e| = \hbar/3$ [8]. This simple calculation illustrates that a large amount of the electron spin has an electromagnetic nature, and exists in the space surrounding the charge distribution. We shall use this idea as a guide to the calculation of the radiative corrections to the Larmor precession. We shall consider a point electron and restrict our calculations to the finite contributions to $\boldsymbol{S}_e$.

Let us return to the case of a neutral atom with a single unpaired electron. The last terms in (2) and (3) are responsible for the electromagnetic energy irradiated by precessing the electron. The precessing magnetic nucleus also emits radiation. However, the power emitted by the nucleus is many orders of magnitude smaller (10^{-18}), and will be neglected.

In a Stern-Gerlach device, the atoms spend a short time interval (10^{-4} sec) crossing the magnetic field region. During this movement the precessing electron generates a time varying angular momentum density, which fills the space surrounding the electron, and generates an additional time dependent angular momentum of electromagnetic nature. It is possible to show that the main contribution to the electromagnetic angular momentum $\Delta\boldsymbol{S}_e$, which is created in the small volume ΔV surrounding the electron, comes from the combination of the first term in (2), with the last term in (3). Therefore, from the standard expression of the angular momentum density we get

$$\Delta\boldsymbol{S}_e \simeq \int_{\Delta V} d^3r \, \frac{\boldsymbol{r}}{4\pi c} \times \left\{ \frac{-e\widehat{\boldsymbol{n}}}{r^2} \times \left[\frac{\widehat{\boldsymbol{n}} \times (\widehat{\boldsymbol{n}} \times \ddot{\boldsymbol{\mu}})}{c^2\, r} \right] \right\} \quad , \tag{5}$$

where the volume $\Delta V = 4\pi(c\Delta t)^3/3$ and $\Delta t \to 0$. The integration in (5) gives

$$\Delta\boldsymbol{S}_e = -\frac{2}{3}\,\frac{e}{c^2}\,\ddot{\boldsymbol{\mu}}\,\Delta t \quad . \tag{6}$$

The total instantaneous variation of the angular momentum, which we denote $\dot{\boldsymbol{S}}$, will be given by

$$\dot{\boldsymbol{S}} \equiv \boldsymbol{\mu} \times \boldsymbol{B} + \frac{\Delta \boldsymbol{S}_e}{\Delta t} = \boldsymbol{\mu} \times \boldsymbol{B} - \frac{2}{3} \frac{e}{c^2} \ddot{\boldsymbol{\mu}} \ . \tag{7}$$

Taking into account the equation (1) the above expression can be written as

$$\dot{\boldsymbol{\mu}} \simeq \frac{e\boldsymbol{B}}{mc} \times \boldsymbol{\mu} + \tau \ddot{\boldsymbol{\mu}} \ , \tag{8}$$

where $\tau = 2e^2/3mc^3 \simeq 6.3 \times 10^{-24}$ sec.

The terms depending on $\dot{\boldsymbol{\mu}}$ in the equations (2) and (3) also contribute to the equation (8). One can show, however, that its contribution is given by $\tau \dot{\boldsymbol{\mu}} \times \ddot{\boldsymbol{\mu}}/mc^2$ being thus much smaller than $\tau \ddot{\boldsymbol{\mu}}$ (see ref. [2]). Another observation, which one can infer from the above derivation (see equations (5), (6) and (7)), is that equation (8) is applicable to the neutral atoms crossing the Stern-Gerlach devices, because the *local* conservation of the angular momentum (used in our derivation) governs the microscopic radiation torque, and the time variation of the vector $\boldsymbol{\mu}(t)$.

The last term in equation (8) will modify the Larmor precession by introducing a variation in the angle θ. In order to calculate this variation we shall neglect the unphysical runaway solutions [6]. According to our Fig. 1 we shall denote

$$\boldsymbol{\mu} = \mu(\sin\theta \cos\phi, \sin\theta \sin\phi, \cos\theta) \ , \tag{9}$$

where $\mu = |\boldsymbol{\mu}|$ is constant.

The Larmor frequency $\omega > 10^{11}\,\mathrm{sec}^{-1}$ for $|\boldsymbol{B}| > 10^4$ gauss. Therefore, we shall assume that $|\ddot{\theta}|\tau \ll \omega$, $|\dot{\theta}| \ll \omega$ and $|\ddot{\phi}|\tau \ll \omega$. According to (8) the first component of the vector $\boldsymbol{\mu}$ obeys the equation $\dot{\mu}_1 = -\omega \mu_2 + \tau \ddot{\mu}_1$.

From this equation we get $\dot{\phi} \simeq \omega$ and

$$\dot{\theta} \simeq -\tau \omega^2 tg\,\theta \ . \tag{10}$$

This simple equation can be integrated giving

$$\cos\theta = \cos\theta_0 \sqrt{1 + tg^2\,\theta_0\,(1 - e^{-2\omega^2\tau t})}\ , \tag{11}$$

where θ_0 is the initial angle. For long times the solution (11) has the remarkable property that $\cos\theta \to +1$ (if $\theta_0 < \pi/2$) and $\cos\theta \to -1$ (if $\theta_0 > \pi/2$). As far as we know this interesting consequence of the radiative corrections was first noticed by A.F. Rañada and M.F. Rañada [2]. We shall see below that, although the variation of the angle θ is small, for the fast particles crossing a Stern-Gerlach device, the incident beam is divided in two outgoing beams by the action of the radiation reaction torque. Notice that $\tau\omega^2 > 1$ for magnetic fields greater than 6×10^4 gauss.

3. SPLITTING OF THE MAXWELL-BOLTZMANN VELOCITY DISTRIBUTION

We shall discuss the details of the motion inside the pole pieces of a Stern-Gerlach magnet by assuming that the magnetic field is given by

$$\boldsymbol{B} = (-\beta x\,,\,0\,,\,B_0 + \beta z)\ , \tag{12}$$

where $\beta = 2 \times 10^5$ gauss/cm [9]. The constant B_0 will take several values within the range 2×10^4 gauss $\leq B_0 \leq 6 \times 10^5$ gauss. The beam is narrow as indicated in the Fig. 2. The width $\Delta z = 0.03\,\mathrm{mm}$ were used in the first experiments [9,10].

The magnetic particles (silver atoms, for instance) move in the direction y with velocity $v_y = v$, distributed according to the Maxwell-Boltzmann law (temperature $T \simeq 1000^{\circ}\,\mathrm{K}$)

$$W(v)\,dv = \frac{2\,v^3\,dv}{\alpha^4}\,e^{-v^2/\alpha^2}\ , \tag{13}$$

where $\alpha^2 = 2kT/M$ so that $v_p = \sqrt{3kT/M}$ is the most probable velocity, and M is the mass of the atom.

The length of the magnetic field region is ℓ and the detecting screen is located at a distance $D > \ell$ as is illustrated in the Fig. 3. We shall consider $\ell = 10\,\mathrm{cm}$ and $D = 50\,\mathrm{cm}$. The above numerical values are typical values considered in the experiments [9–12].

In what follows we shall assume that the particles spend a short time $t = \ell/v_p \simeq 4.83 \times 10^{-4}\,\mathrm{sec}$ [9] in the magnetic field region, so that the quantity $2\omega^2\tau t$ appearing in (11) is small. Therefore, one can approximate $\cos\theta$ by (see Fig. 2 and eq. (11))

$$\cos\theta \simeq \cos\theta_0 \left[1 + \left(\omega^2 \tau\, t\right) tg^2\theta_0\right] \quad . \tag{14}$$

This expression will be used in order to integrate Newton's equations of motion in the interval $0 \leq t \leq \ell/v$.

The accelerations in the x and z directions are given by

$$\dot{v}_x = \frac{\mu\beta\,\beta x_0}{MB}\cos\theta \quad , \tag{15}$$

and

$$\dot{v}_z = \frac{\mu\beta\,B_0}{MB}\cos\theta \quad , \tag{16}$$

where $B = \sqrt{\beta^2 x_0^2 + B_0^2}$. For simplicity we have assumed that the particle enters the magnet in the point $x = x_0$ and $z = 0$. Notice that $\cos\theta$ is a function of time (see (14)).

We shall also consider that these accelerations are small, so that the heavy silver atom has a negligible transversal displacement inside the magnet. Therefore, the components v_z and v_x of the transversal velocity, at the end of the magnetic field region, are given by

$$v_z \simeq \frac{\mu\beta B_0}{MB}\left(\frac{\ell}{v}\cos\theta_0 + \frac{\omega^2\tau}{2}\,\frac{\ell^2}{v^2}\,\frac{\sin^2\theta_0}{\cos\theta_0}\right) \quad , \tag{17}$$

and

$$v_x = \frac{\beta x_0}{B_0} v_z \quad , \tag{18}$$

provided the particle enters the magnet with velocity $v_y = v$ and initial orientation θ_0 (see eq. (14) and Fig. 2).

4. DISTRIBUTION OF PARTICLES ON A DISTANT SCREEN

The screen is located at a distance D after the exit of the magnetic field region (see Fig. 3). Therefore, according to the equations (14), (17) and (18) we have

$$z = v_z \frac{D}{v} \simeq \frac{\mu\beta\ell D}{Mv^2}\,\frac{B_0}{B}\cos\theta_0\left[1 + \xi\, tg^2\theta_0\right] \quad , \tag{19}$$

and

$$x = x_0\left(1 + \frac{\beta z}{B_0}\right) \quad , \tag{20}$$

where

$$\xi \equiv \frac{\omega^2\tau\ell}{2v} \simeq \frac{\omega^2\tau\ell}{2}\sqrt{\frac{M}{3kT}} \quad . \tag{21}$$

In (21) we have replaced v by $\sqrt{3kT/M}$ which is the most probable velocity. These approximations are sufficiently accurate and enables us to calculate more easily the distribution of particles on the screen. Notice that the incident beam is unpolarized (random distribution of the orientation angle θ_0) and the distribution of velocities $v_y = v$ is given by the Maxwell-Boltzmann law (eq. (13)). For the sake of simplicity we shall calculate the distribution for $x = x_0 = 0$. This distribution is defined by

$$G(z) \equiv \int_0^\pi \frac{\sin\theta_0\, d\theta_0}{2} \int_0^\infty \frac{2v^3\, dv}{\alpha^4}\, e^{-v^2/\alpha^2}\,\delta\left[z - \frac{\mu\beta\ell D}{Mv^2}\cos\theta_0\left(1 + \xi\, tg^2\theta_0\right)\right] \quad , \tag{22}$$

because the incident beam is unpolarized. Notice that

$$\int_{-\infty}^{\infty} dz\, G(z) = 1 \quad . \tag{23}$$

The above expression (22) for $G(z)$ is an idealization. It corresponds to assume that collimating slits (see Fig. 2) are arbitrarily narrow. In practice the slits are very narrow, the width Δz being of the order $0.03\,\mathrm{mm}$ [9,10]. The extension of our calculations to the case $\Delta z \neq 0$ is straightforward.

Using eq. (22) one can show that

$$G(z) = \frac{\eta^2}{|z|^3} \int_0^{\pi/2} \sin\theta_0\, d\theta_0 \left(\cos^2\theta_0 + 2\,\xi \sin^2\theta_0\right) \times \exp\left[-\frac{\eta}{|z|}\left(\cos\theta_0 + \xi\,\frac{\sin^2\theta_0}{\cos\theta_0}\right)\right] \tag{24}$$

where

$$\eta \equiv \frac{\mu\,\beta\,\ell\,D}{M\alpha^2} = \frac{\mu\,\beta\,\ell\,D}{2kT} \quad . \tag{25}$$

A convenient form for $G(z)$ is

$$\eta\, G(z) = \int_0^{\eta/|z|} du\, \left[u^2(1-2\xi) + 2\xi\right] \exp\left(-\left[u(1-\xi) + \frac{\xi\,\eta^2}{u\,z^2}\right]\right) \quad . \tag{26}$$

It is also useful the expression for the particular case $\xi = 0$, namely, the case in which the radiation reaction effects are neglected. We obtain

$$\eta\, G_0(z) = \int_0^{\eta/|z|} du\, u^2\, e^{-u} = 2 - \exp\left(-\frac{\eta}{|z|}\right)\left(2 + \frac{2\eta}{|z|} + \frac{\eta^2}{z^2}\right) \quad . \tag{27}$$

5. DISCUSSION

According to the first experimental result obtained by Stern and Gerlach in 1921 (see [9]), the separation on the screen was very small ($\simeq 0.1\,\mathrm{mm}$) because they have considered $D = 0$. More recent experiments consider $D > \ell$. We shall take $\ell = 10\,\mathrm{cm}$ and $D = 50\,\mathrm{cm}$ as typical values [12]. The temperature is $T = 1000^{\circ}\,\mathrm{K}$

and the atomic beam is made of silver atoms for which $M \simeq 1.8 \times 10^{-22}$ g and $\mu = 9.27 \times 10^{-21}$ erg/gauss. According to references [9–11], $\beta = 2 \times 10^5$ gauss/cm and $B_0 = 2 \times 10^4$ gauss. We shall take 2×10^4 gauss $\leq B_0 \leq 6 \times 10^5$ gauss. This is an important information because our parameter ξ (see (20)) depends on the Larmor frequency $\omega = e\,B_0/mc$. Taking into account these numerical values we get $\eta \simeq 3.3$ cm from the expression (25). In the figures below the parameter η is fixed. We shall consider, however, several values of ξ, obtained by varying B_0 in the range indicated above. Therefore, we shall consider some values of ξ within the interval $33 \times 10^{-5} \leq \xi \leq 0.3$.

In the Fig. 4 we show $G_0(z)$, that is, the distribution obtained by neglecting the radiation reaction forces acting upon the magnetic particles crossing the Stern-Gerlach apparatus. This is the well-known result, namely, the image of the central part of the slit shows only the widening generated by the magnetic forces (see (16) and (17)). The beam is not splitted. According to the usual Stern-Gerlach phenomenon it is expected a separation of beam given by the amount [12]

$$\Delta_{SG} = 2\eta \left(1 + \frac{\ell}{2D}\right) \simeq 6.6\,\text{cm} \quad , \tag{28}$$

where η is given by (25). As we said in the introduction, we have neglected the Stern-Gerlach phenomenon in our calculation, in order to clearly identify the signature of the radiation reaction forces.

In our Fig. 5 we show the function $G(z)$ obtained by considering $\xi = 33 \times 10^{-5}$ which corresponds to take $B_0 = 2 \times 10^4$ gauss which is the value used by Stern-Gerlach in the first experiments [9]. The separation generated by the radiation reaction is $\Delta_{RR} \simeq 0.8\,\text{cm}$ being smaller than Δ_{SG} but measurable. In the figures 6 and 7 we show $G(z)$ for $B_0 = 10^5$ gauss and $B_0 = 6 \times 10^5$ gauss. For $B_0 = 10^5$ gauss $\Delta_{RR} \simeq 1.2\,\text{cm}$ and $\Delta_{RR} \simeq 2.8\,\text{cm}$ for $B_0 = 6 \times 10^5$ gauss. In our Fig. 8 we compare $G_0(z)$ with $G(z)$ for $B_0 = 6 \times 10^5$ gauss. From the Fig. 8 we see that, besides the splitting of the original

beam, the radiation reaction torque generates a large widening of the final separated beams (each beam has a width larger than 10 cm). Based on these results, one can conclude that the experimental verification of the effects of the radiation reaction in the Stern-Gerlach devices, is possible using the present day technology. Finally, we would like to suggest, that the radiation reaction effects discussed here, might be relevant to the experimental verification of the Stern-Gerlach effect for electron beams [13].

References

[1] K. Dechoum, H.M. França and C.P. Malta, *Phys. Lett.* **A248** (1998) 93.

[2] Antonio F. Rañada and Manuel F. Rañada, *J. Phys. A: Math. Gen.*, vol. **12** (1979) 1419.

[3] A.V. Barranco, S.A. Brunini, H.M. França, *Phys. Rev.* **A39** (1989) 5492.

[4] J.D. Jackson, "Classical Electrodynamics" (John Wiley & Sons, Inc., New York, 1975) chapter 14 and p. 264.

[5] See ref. [4], chapter 17.

[6] H.M. França, G.C. Marques and A.J. da Silva, *Nuovo Cim.* **48A** (1978) 65.

[7] V.F. Weisskopf, *Phys. Rev.* **56** (1939) 72.

[8] E.P. Tryon, in "Relations between charge, spin, mass, and magnetic moment in classical models for electrons and muons" (unpublished work).

[9] W. Gerlach and O. Stern, *Z. Phys.* **9** (1922) 349; **9** (1922) 353; *Annalen der Physik* **16** (1924) 673.

[10] John B. Taylor, *Phys. Rev.* **28** (1926) 576.

[11] K.F. Smith, "Molecular Beams" (John Wiley & Sons, Inc., London, 1955) chapter IV.

[12] A.P. French and F.F. Taylor, "An Introduction to Quantum Physics" (Norton, New York, 1978) chapter 10.

[13] H. Batelaan, T.J. Gay and J.J. Schwendiman, *Phys. Rev. Lett.* **79** (1997) 4517.

FIGURE CAPTIONS

FIG. 1

The orientation angles of the vector $\boldsymbol{\mu}(t)$ which precesses around the magnetic field $\boldsymbol{B}$.

FIG. 2

Schematic picture of the precession in a non-uniform magnetic field $\boldsymbol{B}$. The initial orientation angle is θ_0. The particles in the beam (shaded area) move with velocity v in the y direction.

FIG. 3

Schematic picture of the Stern-Gerlach type apparatus. The length of the magnetic field region is ℓ and the detecting screen is located at a distance D after the magnet.

FIG. 4

Distribution function $G_0(z)$ calculated by neglecting the radiation reaction (eq. (27)). The parameter $\eta = 3.3\,\mathrm{cm}$ and width of the distribution is $2.4\,\mathrm{cm}$ approximately. In all figures $100 = 1\,\mathrm{cm}$.

FIG. 5

Distribution function $G(z)$ (see eq. (25)) obtained by using $\beta = 2 \times 10^5$ gauss/cm and $B_0 = 2 \times 10^4$ gauss as in the first Stern-Gerlach experiment [9]. The separation generated by the radiation reaction is $\Delta_{RR} \simeq 0.8\,\mathrm{cm}$. The value of the parameter $\eta = 3.3\,\mathrm{cm}$ is the same in all figures. The parameter $\xi = 3.3 \times 10^{-4}$.

FIG. 6

The function $G(z)$ obtained by considering $\xi = 0.08$ ($B_0 = 10^5$ gauss). The separation $\Delta_{RR} \simeq 1.2\,\mathrm{cm}$.

FIG. 7

The function $G(z)$ obtained for $B_0 = 6 \times 10^5$ gauss which corresponds to $\xi \simeq 0.3$. The separation $\Delta_{RR} \simeq 2.8\,\mathrm{cm}$.

FIG. 8

Comparison between $G(z)$, for $B_0 = 6 \times 10^5$ gauss, and $G_0(z)$. The effect of the radiation reaction is very big. We see that, besides the separation of $\Delta_{RR} \simeq 2.8\,\mathrm{cm}$, each beam presents a clear widening, larger than $10\,\mathrm{cm}$.

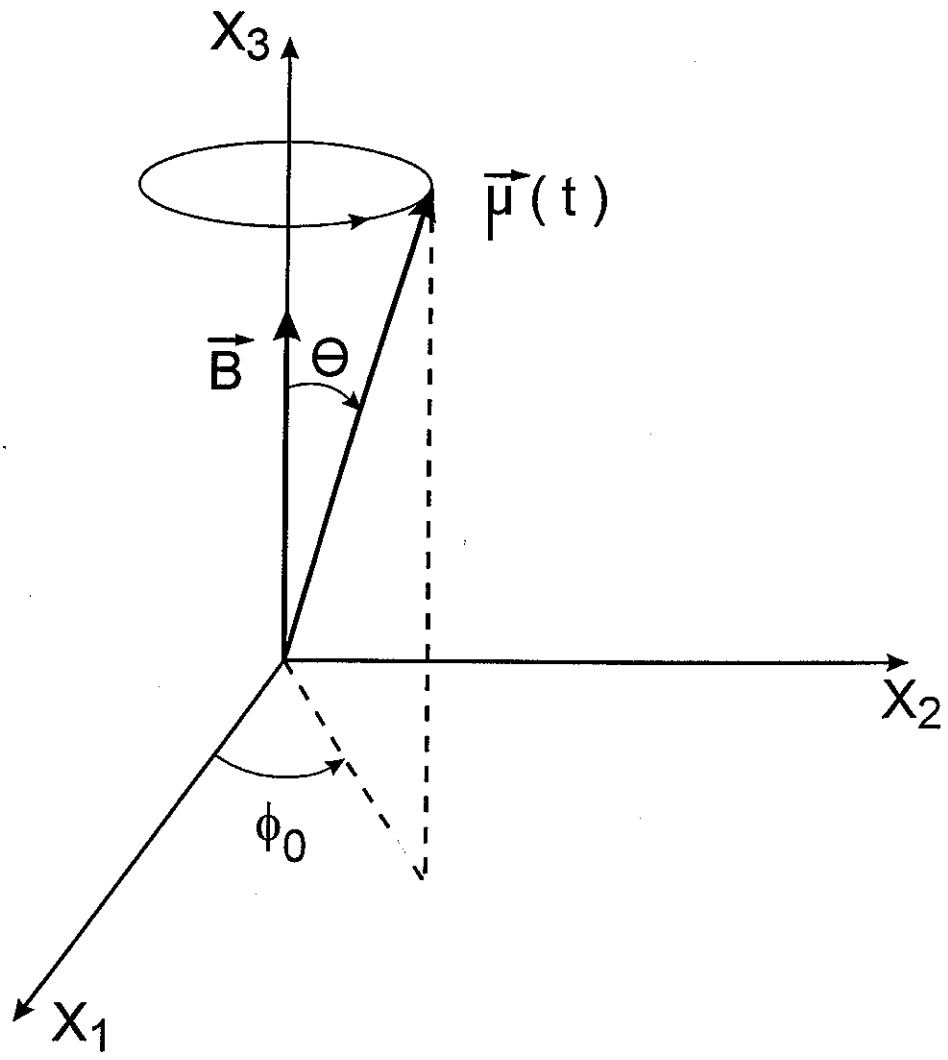

FIG. 1

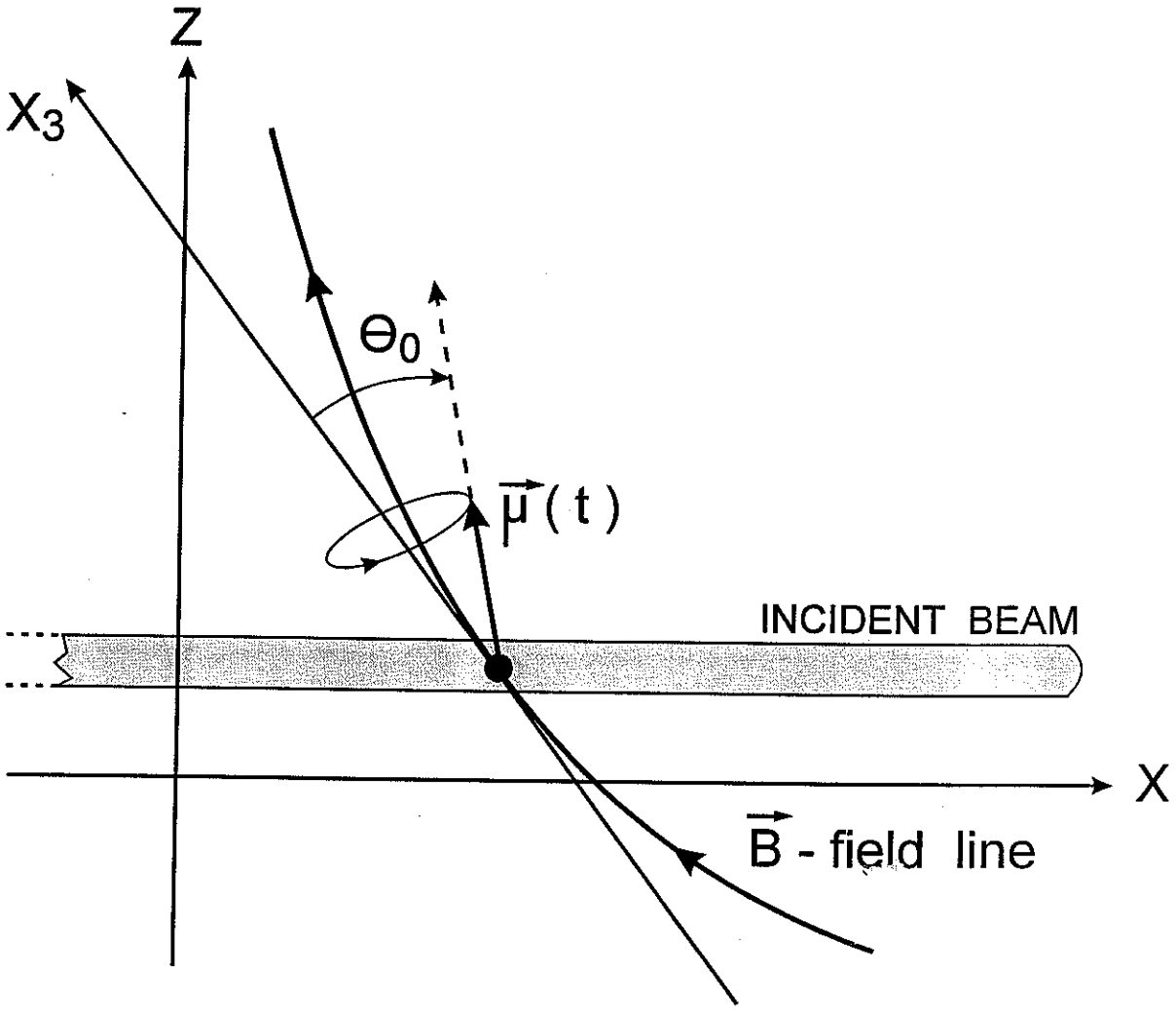

FIG. 2

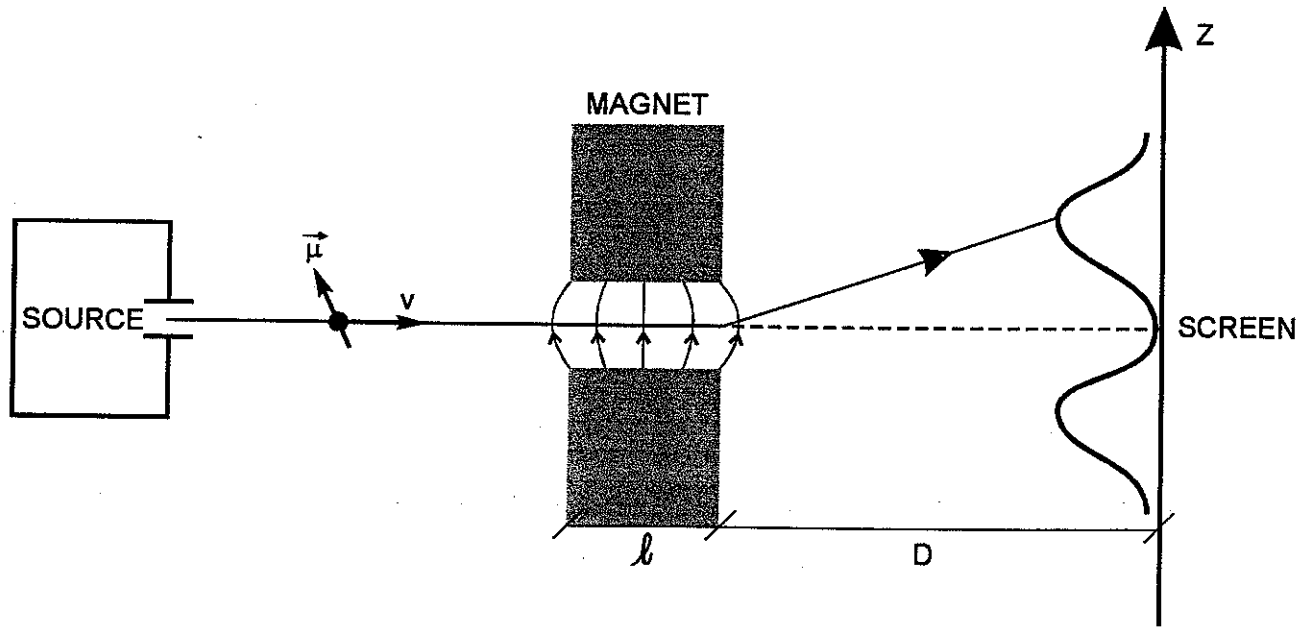

Fig. 3

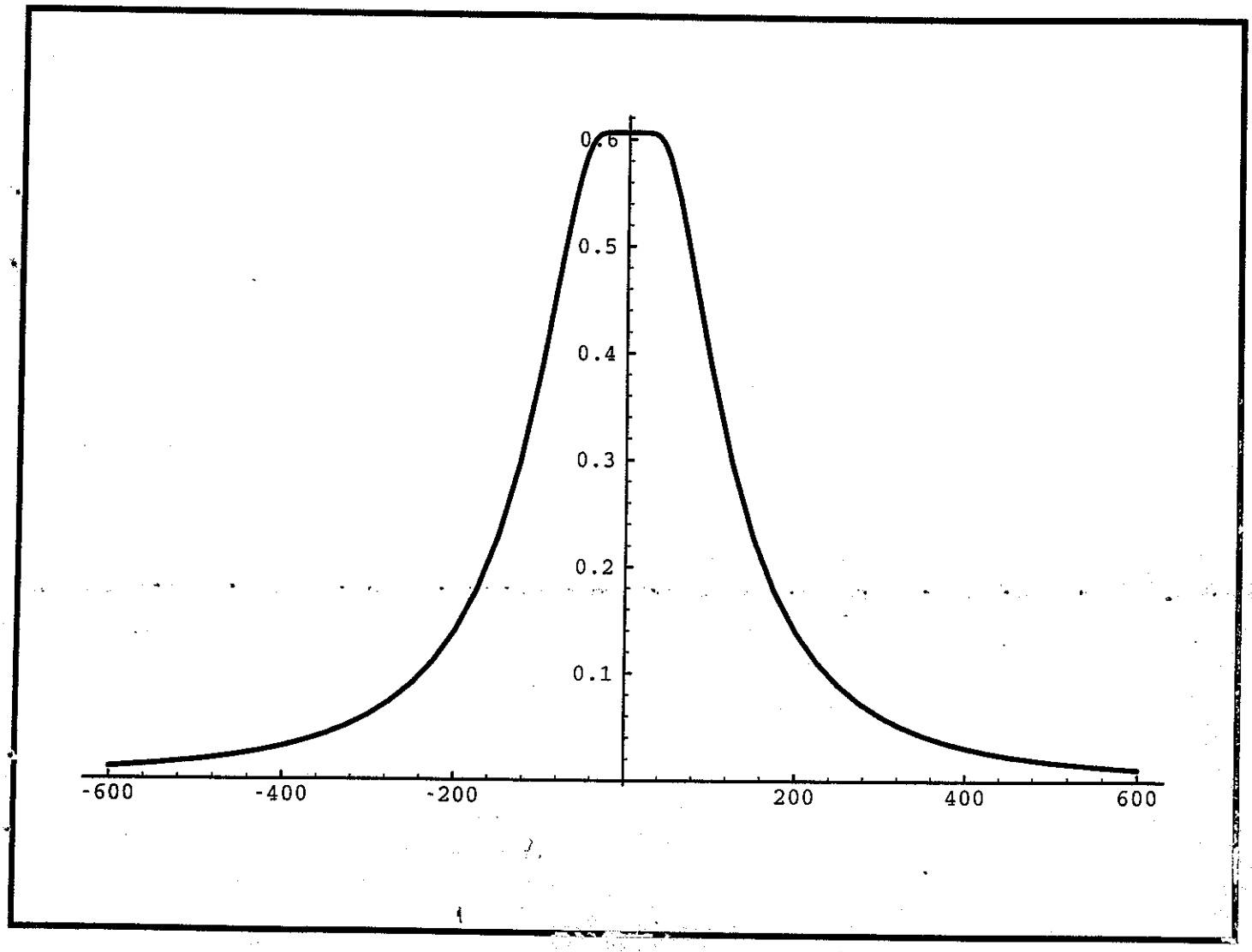

Fig. 4

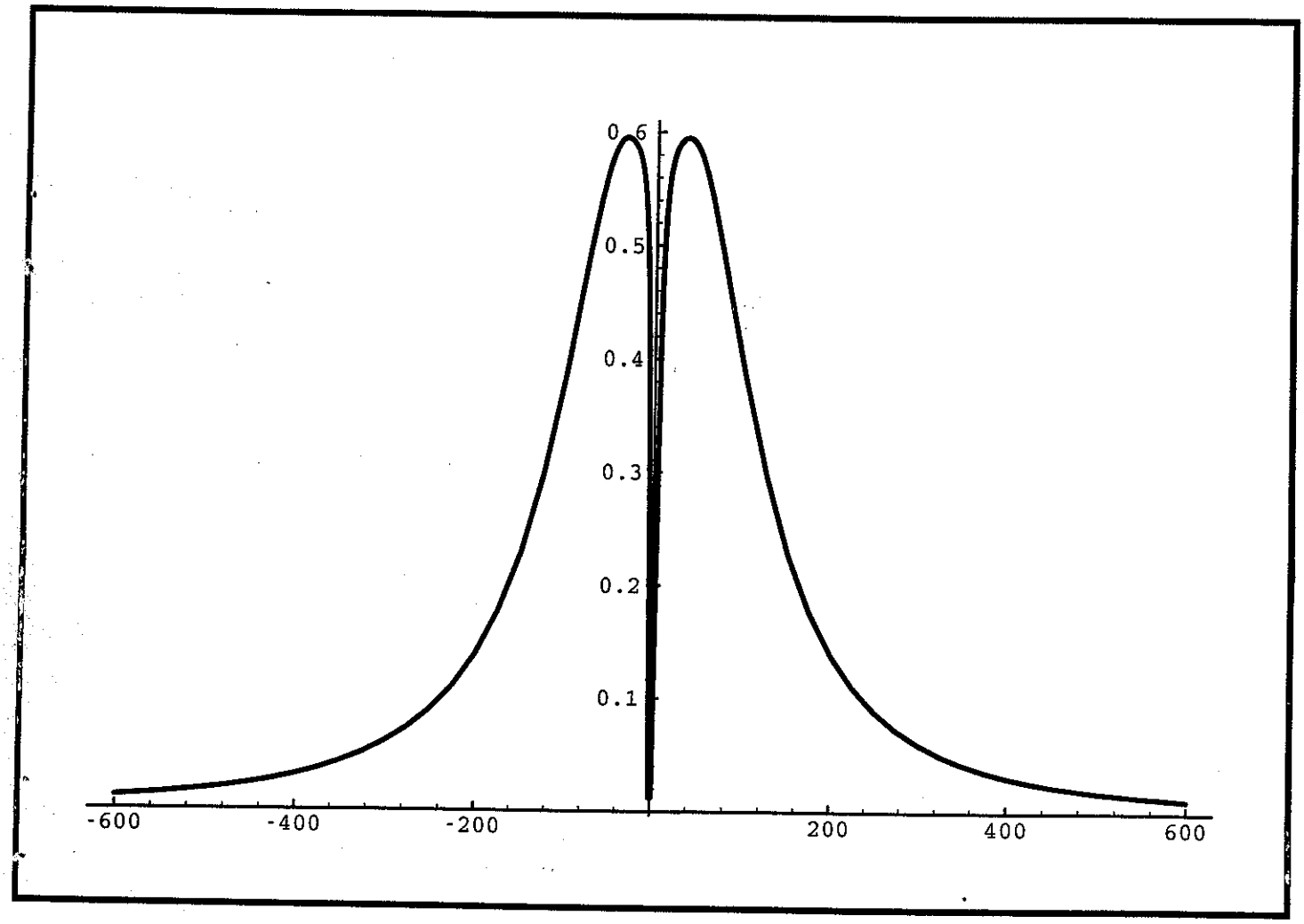

Fig. 5

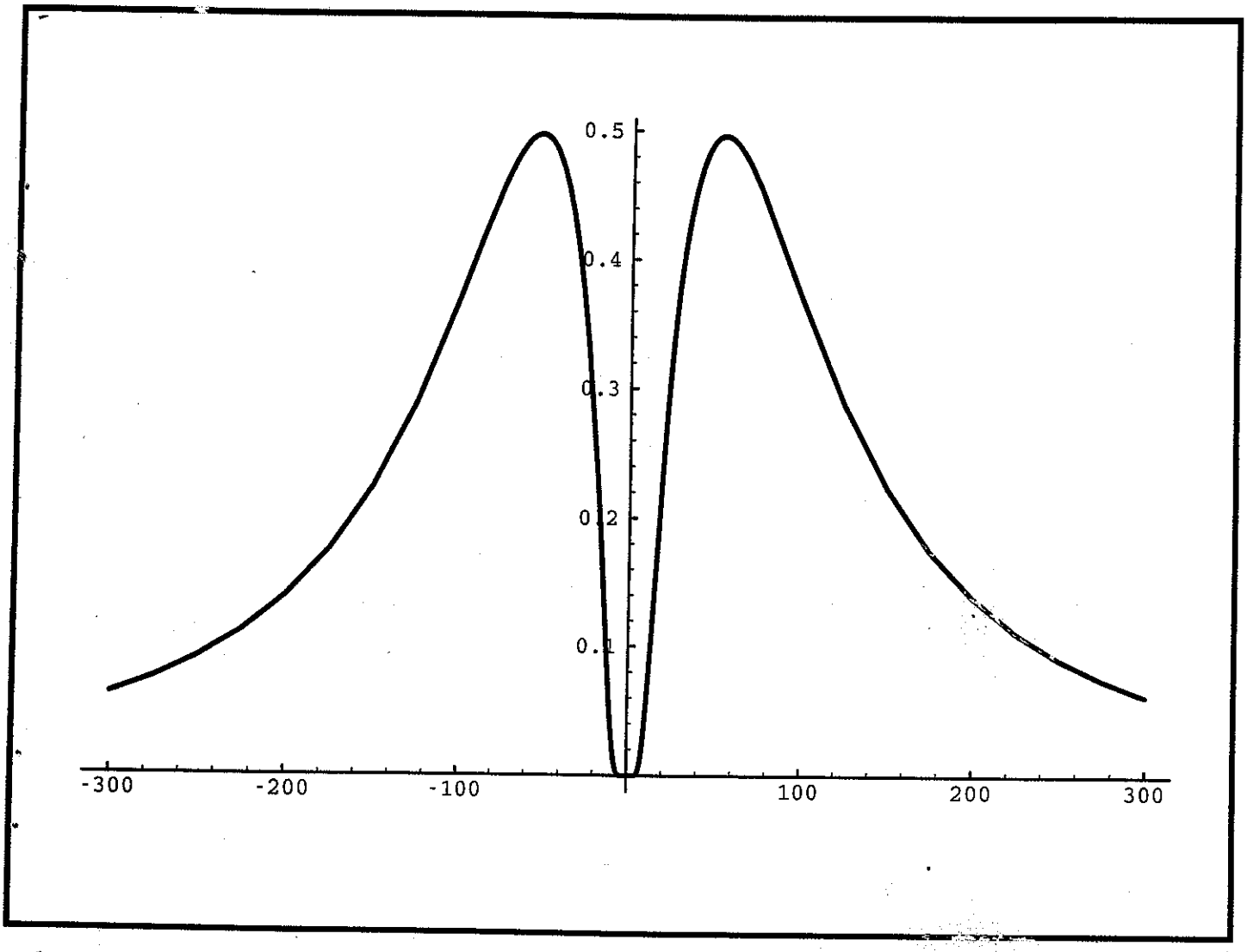

Fig. 6

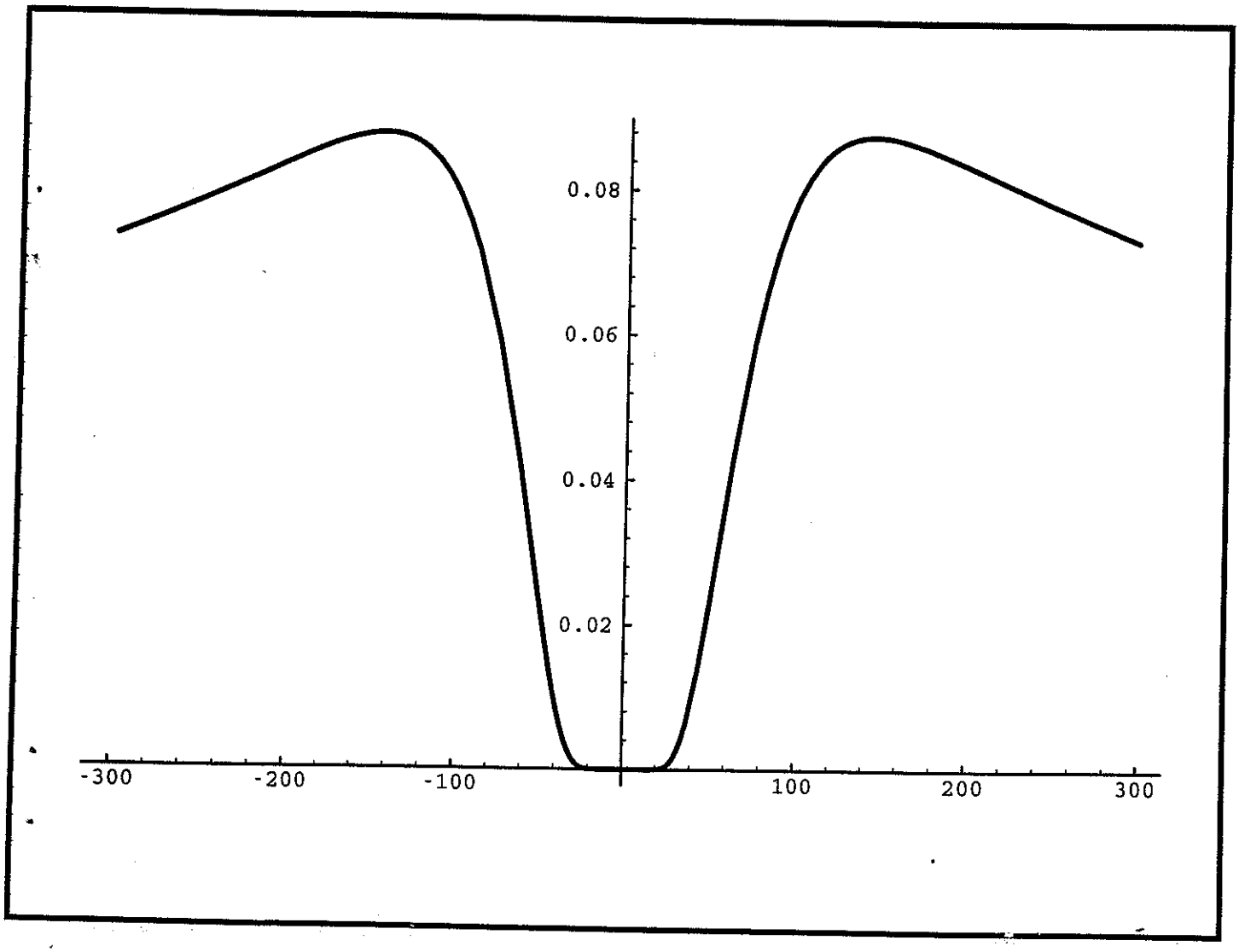

Fig. 7

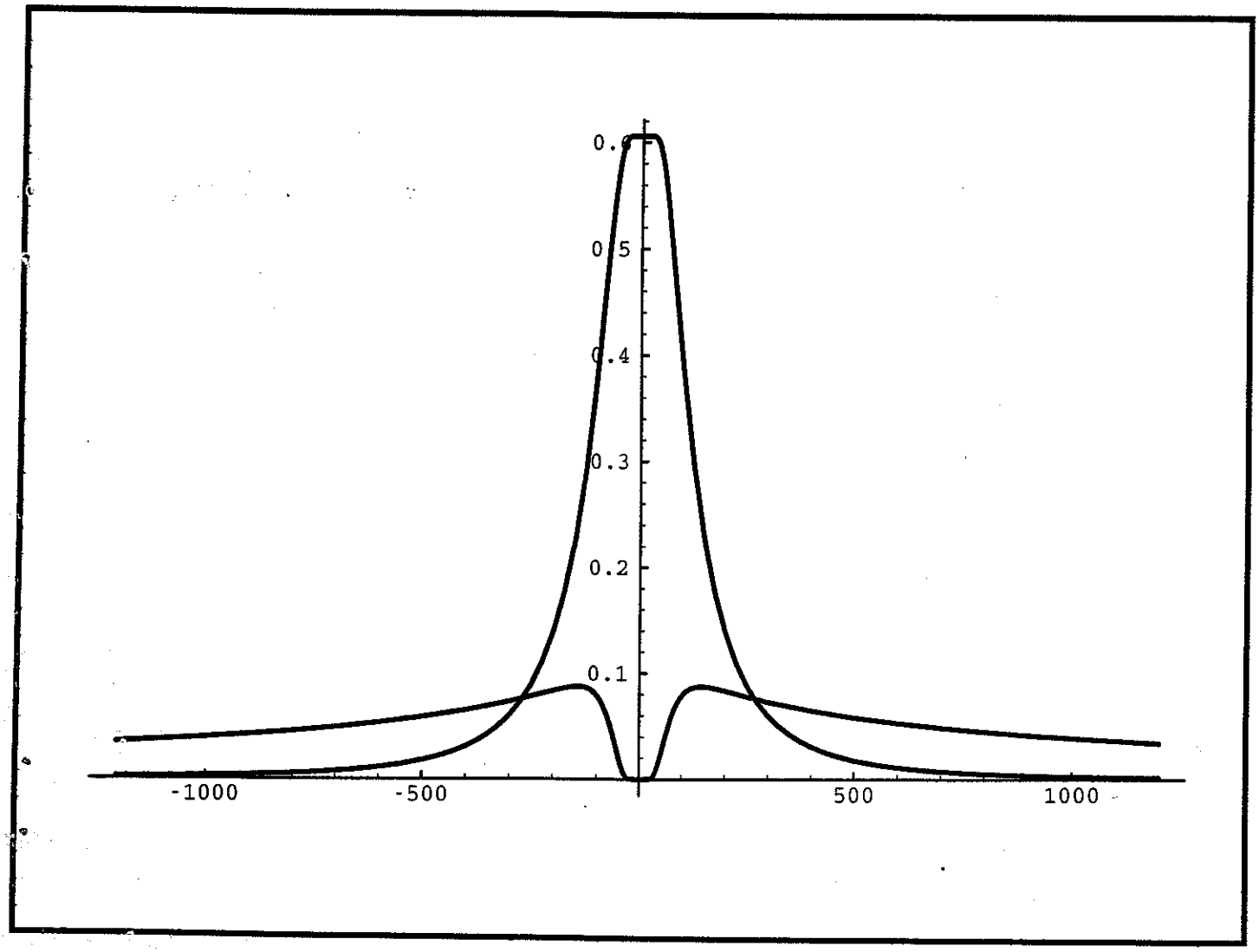

Fig. 8